Heat/mass transfer from surface films to shear flows at arbitrary Peclet numbers

Howard A. Stone[a)]
Department of Applied Mathematics and Theoretical Physics, University of Cambridge, Cambridge CB3 9EW, United Kingdom

(Received 9 December 1988; accepted 4 April 1989)

An efficient numerical method is described for studying the combined conductive and convective transport from a surface film on a planar boundary to a fluid in simple shear flow. Such problems arise most commonly in the use of hot film anemometers, electrochemical shear probes, or in simple models of chemical reactions. The method is illustrated by calculating the total flux (Nusselt number) and variation of the flux along the surface for isothermal circular disks at arbitrary values of the Peclet number (dimensionless shear rate) and is compared with asymptotic results valid at high and low Peclet numbers. The theoretical low Peclet number results of Phillips [Q. J. Mech. Appl. Math. (in press)] lie within 2% of the numerical results for Peclet numbers as high as $P = 2$. At high Peclet numbers, a theoretical estimate for the neglected flux from the edge regions is used, together with the numerical simulations, to propose a correction to the standard one-term asymptotic expression. This approximate relationship remains within 7% of the numerical calculations for Peclet numbers as small as $P = 5$. In addition, results for the total heat transfer as a function of Peclet number are presented for isolated elliptical disks at two orthogonal orientations with respect to the flow and an asymptotic expression for high Peclet numbers is presented for arbitrary disk orientations.

I. INTRODUCTION

An efficient numerical procedure is presented for studying heat or mass transport from two-dimensional surface films to a fluid undergoing a simple shear flow. Both the local flux distribution and the total flux from the film are determined for arbitrary values of the shear rate and the method is illustrated by examining isothermal circular and elliptical surface films.

Transport processes, such as the one studied in this paper, are models of hot film anemometers and electrochemical shear probes, devices that are commonly used to measure wall shear stresses in laminar and turbulent flows[1] and shear stresses in blood flow.[2] In addition, since heat transfer from a surface is a sensitive function of the local fluid motion, in particular, the nature of the macroscopic boundary condition, hot film anemometers have also been used to study wall slip of viscoelastic fluids.[3] Because of the classical character of transport resulting from fluid flow over a planar surface, similar heat and mass transfer problems are found in a variety of other fields, e.g., aeronautics, catalysis, and corrosion. Throughout this paper we will base the discussion on the thermal problem since the mass transfer analog is self-evident.

We consider steady simple shear flow over a solid plane boundary, $\mathbf{u} = (\gamma z, 0, 0)$, where γ is the fluid shear rate. Mounted flush in the insulated boundary ($z = 0$) is a two-dimensional heated surface element that, at least in principle, may be of arbitrary shape (see Fig. 1). The importance of convective compared with conductive transport of heat is measured by the Peclet number P, defined as $P = \gamma l^2/\kappa$, where κ is the thermal diffusivity of the fluid and l is an appropriate characteristic length. It is most often of interest to calculate the flux from the surface for a given prescribed temperature field along the surface or to determine the surface temperature if the heat flux distribution is prescribed. Alternatively, the local flux may be a function of temperature on the film (in situations that involve mass transfer this provides simple models for chemical reactions), in which case the temperature and flux are both unknown *a priori*. The numerical procedure presented here recasts the original problem into an integral equation involving quantities defined on the boundary only and, consequently, solves directly for the unknown surface flux or temperature, thus allowing the study of all three problems just mentioned.

A number of assumptions are implicit in the model problem displayed in Fig. 1. In many cases the actual flow

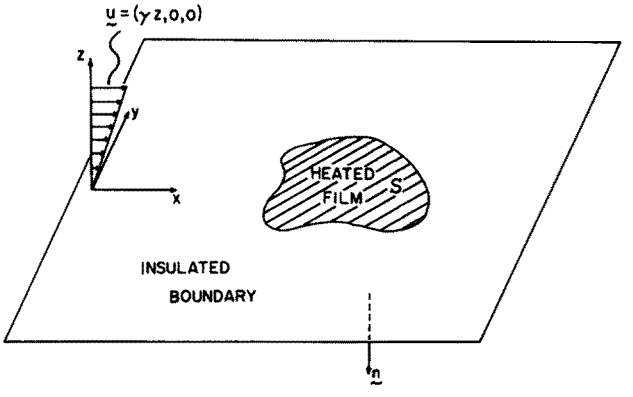

FIG. 1. Schematic of the transport situation: shear flow over a planar boundary containing a heated surface film.

[a)] Present address: Division of Applied Sciences, Pierce Hall, Harvard University, Cambridge, Massachusetts 02138.

 0899-8213/89/071112-11$01.90

situation involves a developing boundary layer as a result of fluid flow over the surface containing the heated element. Provided the temperature variations occur within the momentum boundary layer, generally valid for large values of the Prandtl number ν/κ (ν is the kinematic viscosity), and that the heated area is smaller than the distance characteristic of shear rate changes, it is reasonable to assume that the velocity field is a simple shear flow with a constant shear rate over the surface film. Of course, from the point of view of analysis, it is a major simplification that the fluid mechanics are specified initially. We further assume that the effect of temperature on material properties is negligible and that the surrounding substrate has a very low conductivity. A thorough discussion of these issues is provided by Phillips.[4] The case of a conducting substrate has been treated by Kalumuck,[5] who demonstrated that the primary effect of a finite conductivity substrate was to modify the zero flow heat transfer, but had little influence on the flow-sensitive portion of the flux.

Almost all previous work has been restricted to two-dimensional situations of shear flow (both steady and unsteady) over a heated strip. These studies include a small Peclet number investigation using the method of matched asymptotic expansions[6] and numerical and analytic studies for high Peclet numbers.[7–11] In most applications, however, the surface film is circular, elliptical, or rectangular, so that cross-stream conduction is not negligible and, hence, the transport problem is fully three dimensional. Furthermore, the Peclet number is often $O(1)$. These limitations of two-dimensional theories have often forced the introduction of *ad hoc* assumptions during the design of hot film anemometers or electrochemical shear probes (e.g., Hanratty and Campbell[1]).

Recent studies of Phillips[4] and Kalumuck[5] have focused on the three-dimensional problem. Phillips presents an analytic investigation of heat transfer at low Peclet numbers from isothermal circular disk-shaped films using the method of matched asymptotic expansions. The low Peclet number results are compared with our numerical calculations in Sec. IV and are shown to agree within 2% up to $P = 2$. At high Peclet numbers, Phillips examines the central section and leading, side, and trailing edges of the circular disk. However, because of the complexity of the analysis, Phillips is only able to calculate the first term in an expansion for the total flux (a result previously obtained by Reiss and Hanratty[12] who only considered the flux resulting from the thermal boundary layer that develops above the disk), although an order-of-magnitude estimate is provided for the neglected flux from the edge regions. In Sec. IV, we will use this error estimate, together with the numerical results, to develop a correction to the asymptotic expression for the total heat flux. We will find that the high Peclet number asymptote lies within 5% of the numerical calculations when $P \approx 400.0$. In addition, past investigations in conjunction with Phillips' work give insight into the variation of the heat flux with position along the disk, which is valuable to this numerical study since regions of large local flux must be resolved accurately.

Kalumuck assumes that a uniform flux distribution on the film is prescribed and solves for the temperature field using Fourier transforms, which, because of their complexity, are inverted numerically. The work examines rectangular films for a wide range of Peclet numbers and demonstrates the importance of heat flux to the surrounding substrate. In addition, previous theoretical and experimental studies are well summarized, and relevant operating conditions that arise in the application of hot film anemometry are discussed.

In this paper we extend the work of Phillips and complement the work of Kalumuck by calculating the flux distribution and total flux for isothermal films. The method is illustrated by studying circular disks at Peclet numbers $0.001 \leqslant P \leqslant 400.0$. In addition, we present results for elliptical disks at different orientations to the mean flow, thus allowing an estimate to be made of the errors produced by the misalignment of the probe with the flow. The case of chemical reaction at the surface, a question posed by Hanratty and Campbell,[1] will be discussed in a future communication. The net result of this investigation is an improved quantitative understanding of the dependence of heat transfer on shear rate for steady flows.

General remarks about physical features of the transport problem. Before presenting the mathematical formulation and the associated numerical method, we review some general features of earlier work on the two-dimensional (2-D) and three-dimensional (3-D)problems. These previous studies provide valuable physical insight that will be useful to the implementation of the numerical procedure.

For an isothermal film imbedded in an otherwise insulating surface, the heat flux undergoes a jump discontinuity at the film boundary. In the case of conduction ($P = 0$) from a circular disk of radius a the flux distribution q as a function of radial position r along the heated surface can be evaluated analytically (e.g., Jackson[13]) and has the dimensionless form

$$q = 2/\pi\sqrt{1 - r^2}. \tag{1}$$

This square root singularity is characteristic of local conduction (i.e., solutions of Laplace's equation) in the vicinity of a boundary where the heat flux suffers a jump discontinuity, though in the more general situation discussed here, the appropriate characteristic length scale is the streamwise length of the heated film. Nevertheless, even in the presence of convective transport, we still expect the flux sufficiently close to the edge to display this square root behavior. At low Peclet numbers, these large fluxes in the neighborhood of the edge give rise to a significant contribution to the total flux and, hence, numerical resolution of these large fluxes will be important near the boundary.

At high Peclet numbers, a thermal boundary layer develops above the plate. We expect a balance of conduction normal to the plate and streamwise convection to produce a thermal boundary layer with thickness $O(P^{-1/3})$, so that the total flux from the central portion of the heated element will be $O(P^{1/3})$. This corresponds to the classic boundary layer solution of Leveque.[14] Near the edges, local conduction will be important in all three directions so that there will be a thin region on the film $O(P^{-1/2})$ where the thickness of the ther-

mal boundary layer is also $O(P^{-1/2})$. This will produce an $O(1)$ flux. Although qualitatively correct, this slightly overestimates the actual contribution from the edge regions, which Springer[10] and Phillips[4] find to be $O(P^{-1/6})$. Consequently, the thin regions of large flux resulting from the square root singularity make a less significant contribution to the total heat flux at high Peclet numbers.

As an aside, at high Peclet numbers, if the macroscopic boundary condition is one of slip (so that $u_x = \text{const}$ at $z = 0$), then the thin thermal boundary layer has thickness $O(P^{-1/2})$ giving rise to a flux $O(P^{1/2})$. This is much larger than the $O(P^{1/3})$ flux resulting from the no-slip boundary condition.[3]

II. PROBLEM FORMULATION

At steady state the temperature distribution in the fluid is governed by the convective-diffusion equation, which in dimensionless form is

$$\nabla^2 T - Pz\frac{\partial T}{\partial x} = 0. \tag{2}$$

The (mixed-type) boundary conditions are

$$\mathbf{n}\cdot\nabla T = 0, \quad \text{for } \mathbf{x}_s \notin S,$$

$$T = 1, \quad \text{for } \mathbf{x}_s \in S,$$

$$T \to 0, \quad \text{as } |\mathbf{x}| \to \infty,$$

where $\mathbf{x}_s$ is a position vector lying in the plane, S is the heated film, and $\mathbf{n}$ is the unit outward normal (Fig. 1). The goal of this study is to determine, as a function of Peclet number, the dimensionless local heat flux *from* the heated film *to* the fluid, $q = \mathbf{n}\cdot\nabla T$[15] and the total heat flux, or Nusselt number N, from the surface film

$$N = \int_S \mathbf{n}\cdot\nabla T\, dS. \tag{3}$$

Because the velocity field is specified, we can recast the differential equation into an integral equation involving quantities (unknown flux, temperature) on the planar boundary only. Introducing a Green's function $G(\mathbf{x}_s,\xi;P)$, using Eq. (2) and Green's theorem yields

$$T(\mathbf{x}_s) = \int_S \mathbf{n}\cdot\nabla T(\xi) G(\mathbf{x}_s,\xi;P)\, dS_\xi, \tag{4}$$

where ξ represents the integration variable and integration is limited to the heated surface S only. Physically, G represents the response (temperature) at $\mathbf{x}_s$ resulting from a heat source at ξ of strength $\mathbf{n}\cdot\nabla T$ (the local heat flux). Because of the imposed flow, G is *not* symmetric [see Eq. (7) below]. If G is known and the temperature distribution on the film is specified, (4) is an integral equation of the first kind for the heat flux. This integral equation can be solved numerically in a straightforward manner to yield the heat flux distribution for a variety of shapes of the surface film and we take this equation as the starting point for the numerical work described below.

Compared to finite-difference solutions that require discretization of the entire 3-D domain, representing the solution via a surface integral reduces the dimensionality of the problem, thus offering a substantial simplicity and a significant savings in computation time. The method described here falls under the general category of boundary integral methods, which have been applied to many heat conduction problems.[16]

The Green's function G satisfies the adjoint problem

$$\nabla_\xi^2 G + Pz\frac{\partial G}{\partial x} = 0, \tag{5}$$

subject to the boundary conditions

$$\mathbf{n}\cdot\nabla G = \delta(\mathbf{x}_s - \xi),$$

$$|G| \to 0, \quad \text{as } |\xi| \to \infty.$$

This corresponds to the case of a point source, located on an adiabatic wall, in a shear flow. We note that the Peclet number dependence can be eliminated by rescaling all lengths so that

$$G(\mathbf{x}_s,\xi;P) = P^{1/2} H(P^{1/2}\mathbf{x}_s, P^{1/2}\xi) \tag{6}$$

and the "universal" function $H(\bar{\mathbf{x}}_s,\bar{\xi}) = G(\mathbf{x}_s,\xi;1)$ can be evaluated, in principle, once and used for calculations at arbitrary Peclet number. We present the functional form of H in Sec. III. In this study we find it convenient to retain P as shown in (5) and simply generate an approximation to G for each Peclet number desired.

The solution of (5) can be accomplished using a two-dimensional Fourier transform, although the inversion cannot be performed analytically. This yields

$$G(\mathbf{x}_s,\xi;P) = -\frac{1}{(2\pi)^2}\int_{-\infty}^{\infty}\int_{-\infty}^{\infty} e^{-i\boldsymbol{\lambda}\cdot(\xi-\mathbf{x}_s)} \times \frac{\mathrm{Ai}(s)}{(iP\lambda_x)^{1/3}\mathrm{Ai}'(s)}\, d\lambda_x\, d\lambda_y, \tag{7}$$

where $s = (\lambda_x^2 + \lambda_y^2)/(iP\lambda_x)^{2/3}$, $\boldsymbol{\lambda} = (\lambda_x,\lambda_y)$, and Ai and Ai' are the Airy function and its first derivative.

It proves convenient and very efficient numerically to separate the conductive ($P = 0$) contribution to G and write

$$G(\mathbf{x}_s,\xi;P) = [1/(2\pi)^2]\,[2\pi/|\mathbf{x}_s - \xi| + g(\mathbf{x}_s,\xi;P)]. \tag{8}$$

The function g from which, if desired, the dependence on P can be eliminated by rescaling as in Eq. (6), is given by

$$g(\mathbf{x}_s,\xi;P) = -\int_{-\infty}^{\infty}\int_{-\infty}^{\infty} e^{-i\boldsymbol{\lambda}\cdot(\xi-\mathbf{x}_s)} \times \left[\frac{\mathrm{Ai}(s)}{(iP\lambda_x)^{1/3}\mathrm{Ai}'(s)} + \frac{1}{\sqrt{\lambda_x^2+\lambda_y^2}}\right] d\lambda_x\, d\lambda_y. \tag{9}$$

In the next two sections we discuss the numerical integration to produce a tabular representation of g (and hence G) and the use of the Green's function to solve for the heat flux distribution from (4).

III. NUMERICAL IMPLEMENTATION

A. Numerical determination of the Green's function

In this section we discuss the numerical evaluation of the function g defined by Eq. (9). Once evaluated for a particular value of the Peclet number, the tabulated function g can be used in the numerical solution of (4) for any geometry of the surface film. As mentioned in Sec. II, although the basic form of the function is invariant with respect to

changes of the Peclet number, as a result of the discrete nature of the numerical approximation, it is convenient in this study to retain dependence on P.

The numerical solution of the inverse Fourier transform [Eq. (9)] is approximated by performing a two-dimensional fast Fourier transform (FFT) (e.g., see Brigham[17] or Press, *et al.*[18]). This produces a table of g values at equally spaced points. In such a discrete approximation of a continuous function, it is necessary to specify in each direction both the sampling frequency ($\delta_i, i = x,y$) and the maximum frequency ($\lambda_i^{\max}$) to be sampled in λ space. These are related to the number of points utilized in the discretization M_i and the sampling interval Δ_i in $\mathbf{x}$ space by $\Delta_i = \pi/\lambda_i^{\max}$ and $M_i = 2\pi/\delta_i\,\Delta_i$. In general, additional resolution is needed in the flow direction and at high Peclet numbers, where a long thermal wake extends downstream of the point source, it is necessary to sample large values of $|\lambda|$. This makes numerical calculation of the Green's function more difficult for large Peclet numbers. Typical values of the finite Fourier transform parameters M_i, Δ_i are reported in Table I where the values of Δ_i have been chosen purposely small so that g is known on a fine grid for use in the numerical solution of the integral equation (4). Notice also that, for example, in the case of a circular disk, it is only necessary to retain values of g such that $|\mathbf{x}_s - \xi| \leqslant 2.0$. This restriction on values of $|\mathbf{x}_s - \xi|$ also allows a considerable savings in computer storage to be gained when performing the 2-D FFT.

Straightforward application of the 2-D FFT is rather inaccurate because of the rapid variation of the integrand near the singularity $|\lambda| \to 0$. Since the finite Fourier transform is equivalent from the point of view of numerical integration to a trapezoidal approximation, in a region around the origin (typically extending to $10\,\delta_i$), the trapezoidal approximation of g is subtracted and an accurate Gaussian integration is performed. In the immediate neighborhood of the origin $\lambda = 0$, the integrand is singular (but, nevertheless, is integrable) and is treated analytically by integrating over a circular region of radius ϵ, as described in the Appendix. This small region makes a contribution $-2\pi\epsilon + \hat{c}(\epsilon^5/P)^{1/3}$, where $\hat{c}$ is also given in the Appendix. Typically we choose $\epsilon = 0.01$. With this procedure, varying the FFT parameters about those shown in Table I produce variations in g that appear to be 1%–2%. Computation times on a SUN 3-50 workstation vary widely depending on the values $|\mathbf{x}_s - \xi|$ of interest and the resolution desired. Typically a few minutes are required to calculate the 2-D FFT, although, for high resolutions and large values of $|\mathbf{x}_s - \xi|$ much longer times of an hour or two may be spent performing the correction using the trapezoidal/Gaussian integration discussed above.

Calculation of the Airy function $\mathrm{Ai}(z)$ and its first derivative are accomplished using a power series for small arguments ($z < c$) and continuing the series until the absolute error is less than 10^{-6}. For large arguments ($z > c$) an asymptotic expansion is used[19] and terms are retained until the series begins to diverge. Typically we choose $c = 3.6$. All the calculations described above are performed in single precision, except for the Fourier inversion, which is performed using double precision.

TABLE I. Parameters for 2-D fast Fourier transform.

P	0.01	1.0	100.0
$M_{x,y}$[a]	256	512	1024
$\Delta_{x,y}$	0.2	0.1	0.01

[a] Generally FFT routines utilize values of M_i that are powers of 2.

As discussed in Sec. II, the Peclet number dependence of the Green's function G can be eliminated via rescaling so that it suffices to illustrate the function $H(x,y) = G(x,y;1)$. This function physically represents the thermal field on a planar boundary resulting from a point source located at the origin in the presence of a shear flow and is illustrated in Fig. 2. The solid lines indicate the wall temperature field as a function of x at four different transverse (y) positions. The dashed lines represent the conduction ($P = 0$) solution at similar transverse positions. Because G satisfies the adjoint problem, the long thermal wake is in the $-x$ direction. The effect of flowing cold fluid past the point heat source is clearly to cool the boundary significantly on the upstream side of the source and also has a noticeable effect in cooling the downstream wake region.

B. Numerical solution of the integral equation

With the Green's function determined, we turn our attention to the solution of Eq. (4), which yields the heat flux distribution over the heated region. For clarity in the discussion below, we assume that the heated film is circular with the radius chosen as the characteristic length $l = a$.

There are two principle features of the numerical solution of such integral equations: (1) discretization of the heated area and (2) representation of the unknown heat flux over an element of the surface. The surface is first discretized by subdividing the circular disk into concentric circles (similarly, the elliptical disk is divided into concentric ellipses) and equally subdividing the angular direction as shown in

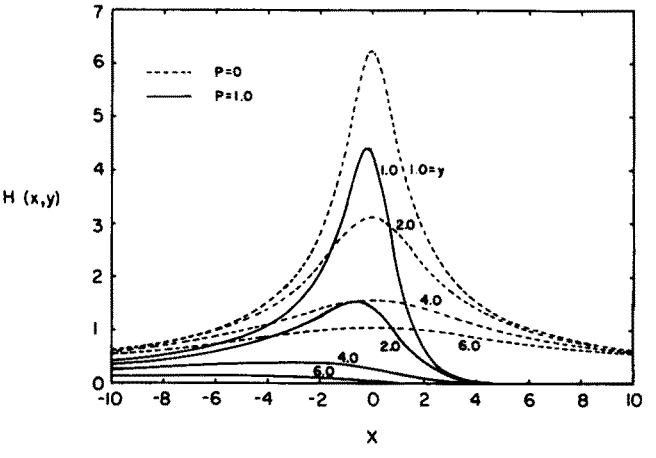

FIG. 2. Wall temperature profiles for a point heat source imbedded in a wall. Solid lines correspond to the numerical results for $P = 1, H(x,y) = G(x,y;1)$ at transverse y positions $y = 1.0, 2.0, 4.0$, and 6.0 and the dashed lines are the conduction solution ($P = 0$) at the same transverse y positions. Since the Green's function satisfies the adjoint problem, the thermal wake is in the $-x$ direction.

Fig. 3, thereby producing n subelements, S_j, $j=1,\ldots,2n$. Equation (4) is then written in the equivalent form

$$T(\mathbf{x}_s)=\sum_{j=1}^{2n}\int_{S_j} q(\xi)G(\mathbf{x}_s,\xi)dS_\xi. \tag{10}$$

We consider three alternative methods for representing the unknown heat flux distribution q_j over surface element j:(i) $q_j=\text{const}=\bar{q}_j$, (ii) $q_j=q_c+\bar{q}_j$, and (iii) $q_j=\bar{q}_j/\sqrt{1-r^2}$, where q_c is the conduction solution ($P=0$) and is known exactly for circular and elliptical disks (Landau and Lifshitz[20]). The $\bar{q}_j$ are assumed constant over element j. Representations (ii) and (iii) build the square root singularity directly into the calculation. In general, all three representations yield quantitatively good results, even though only equal radial and angular spacing of the elements have been employed (see Sec. IV A). Because of symmetry about the flow direction, it is only necessary to determine the unknowns in the upper xy half-plane so that the number of unknowns is halved. Typically, the angular and radial directions are each subdivided into 10–15 elements so that $n\approx 100$–200.

Writing Eq. (10) for node points placed at the center of each element produces the linear system

$$\mathbf{A}\cdot\bar{\mathbf{q}}=\mathbf{b}, \tag{11}$$

where $\mathbf{b}$ and $\mathbf{A}$ are known and the vector of unknowns $\bar{\mathbf{q}}$ is determined by inverting the $n\times n$ matrix $\mathbf{A}$ using standard LU decomposition.[18] The elements of $\mathbf{b}$ and $\mathbf{A}$ for the different computational methods are listed in Table II. The elements A_{ij} may be interpreted as representing the "interaction" of surface element i with surface element j. The diagonal elements of $\mathbf{A}$ involve integration of a singular kernel resulting from the $1/|\mathbf{x}_s-\xi|$ term in Eq. (8). This singularity is handled in a straightforward manner by analytically integrating over a polygonal element containing the singularity and numerically integrating over the remainder of the element away from the singularity.

The calculations described in this section, which typically require several minutes of computation time, are performed in single precision and integration is performed using four point Gauss quadrature. Values of g that arise when computing the elements of $\mathbf{A}$ are determined from the tabulated results described in Sec. III using linear interpolation, which proves to be sufficiently accurate for this work. An alternative procedure that may prove useful in future studies is to generate a single, high resolution representation for g at $P=1$ and then use a high accuracy curve-fitting procedure together with the $P^{1/2}$ scaling discussed in Sec. II [Eq. (6)] to generate a single table of g values for use at all Peclet numbers.

TABLE II. The elements of $\mathbf{b}$ and $\mathbf{A}$. Here S_j^* is the surface element on $y<0$ obtained by reflection about the x axis. In addition, G_{ij} or g_{ij} denotes integration over element S_j or S_j^* with evaluation at node point $\mathbf{x}_{s_i}$.

Method	b_i	A_{ij}
(i)	1	$\int_{S_j+S_j^*} G_{ij}\,dS$
(ii)[a]	$\frac{1}{(2\pi)^2}\Sigma_j g_{ij}q_c\,dS$	$\int_{S_j+S_j^*} G_{ij}\,dS$
(iii)	1	$\int_{S_j+S_j^*}\frac{G_{ij}}{\sqrt{1-r^2}}\,dS$

[a] We have made use of the fact that the Green's function for isothermal films satisfies $(1/2\pi)\int_S[q_c(\xi)/|\mathbf{x}_s-\xi|]dS_\xi=1$.

IV. NUMERICAL RESULTS: CIRCULAR FILMS

A. Comparison of different numerical approximations

The numerical procedure outlined above has been tested by comparing with analytical results where possible and by increasing numerical resolution. In Figs. 4(a)–4(d) we present calculations that are typical of the performance of the different methods. Figure 4(a) shows the heat flux distribution over the leading edge in the case $P=1.0$, calculated using method (i) with several different surface subdivisions (in each case the reported radial and angular subdivisions are equally spaced and only the fineness of the grid is varied). The total heat flux (Nusselt number) for each simulation is reported in the inset. Figures 4(b) and 4(c) show similar calculations for methods (ii) and (iii), respectively, and Fig. 4(d) compares the different methods with the same degree of surface resolution. In general, all three methods perform adequately and even method (i) is capable of crudely resolving the large fluxes near the disk

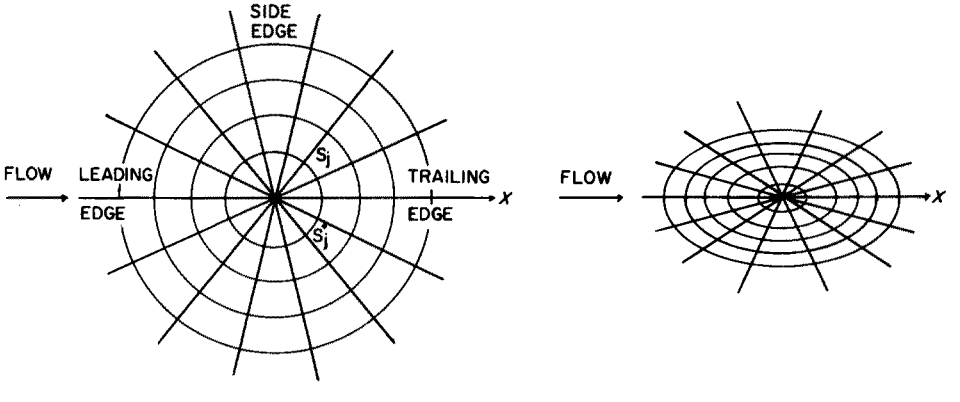

FIG. 3. The discretization of circular and elliptical disks.

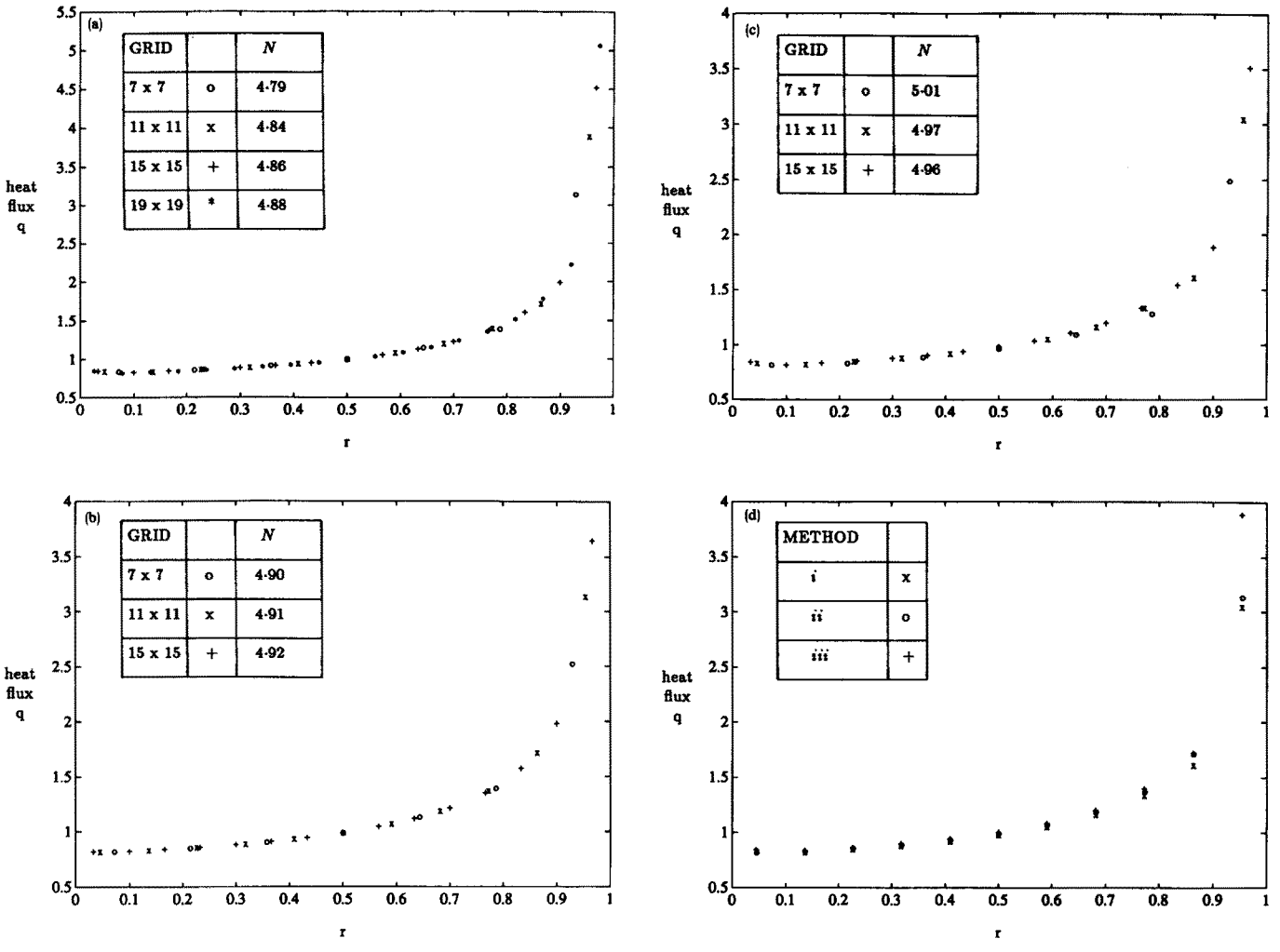

FIG. 4. A comparison of different numerical approximations for representing the heat flux distribution over the leading edge; $P = 1$. (a) method (i); (b) method (ii); (c) method (iii); and (d) the comparison of methods (i)–(iii) using the same surface discretization.

edge. We judge method (ii) to be more accurate for a given number of node points as the flux distributions are smoother and the variation in the calculated total heat flux is smaller as the resolution is increased.

The results reported below all use method (ii) of Sec. III for representing the variation of the local heat flux. In these calculations the disk is subdivided into 11 equally spaced radial and angular elements.

B. Heat flux distribution over the disk as a function of Peclet number

In Figs. 5(a)–5(c) the radial variation of the heat flux is illustrated at three different angular positions on the disk for Peclet numbers $P = 0.01$, 1.0, and 100.0. In each case the symbols *, +, and × correspond to the leading, side, and trailing edge regions, respectively (see Fig. 3). The solid line is the analytic result for conduction, $P = 0.0$ [Eq. (1)].

As expected, at low Peclet numbers, Fig. 5(a), the conduction solution remains within a few percent of the numerically calculated fluxes and there is almost no noticeable difference between the leading, side, and trailing regions. Furthermore, over much of the central region of the disk, there is only a small variation in the flux. The distribution illustrates the square root singularity, which, of course, is not surprising since it has been incorporated into the numerical scheme in order to capture the large flux variations that occur in the vicinity of the edges.

As the Peclet number is increased to $P = 1.0$ [Fig. 5(b)] the heat flux distribution is seen to vary significantly over different regions of the disk. The flux profile, though, is still similar to the conduction solution. At this moderate value of the Peclet number, there is an increased heat transfer over the leading edge of the heated film, such that the fluxes at the front of the disk are larger than those at the trailing edge by almost a factor of 2.

At very high values of the Peclet number, $P = 100.0$, the heat flux is much higher over the leading edge than the trailing edge. In Fig. 5(c), following the asterisks from $r = 1 \rightarrow 0$ and then the × symbols from $r = 0 \rightarrow 1$ illustrates the basically monotonic decrease of the heat flux over the central portion of the disk, until very close to the trailing edge. It is clear that this is due to the preheating effect of the leading edge, which raises the temperature of the cold fluid suffi-

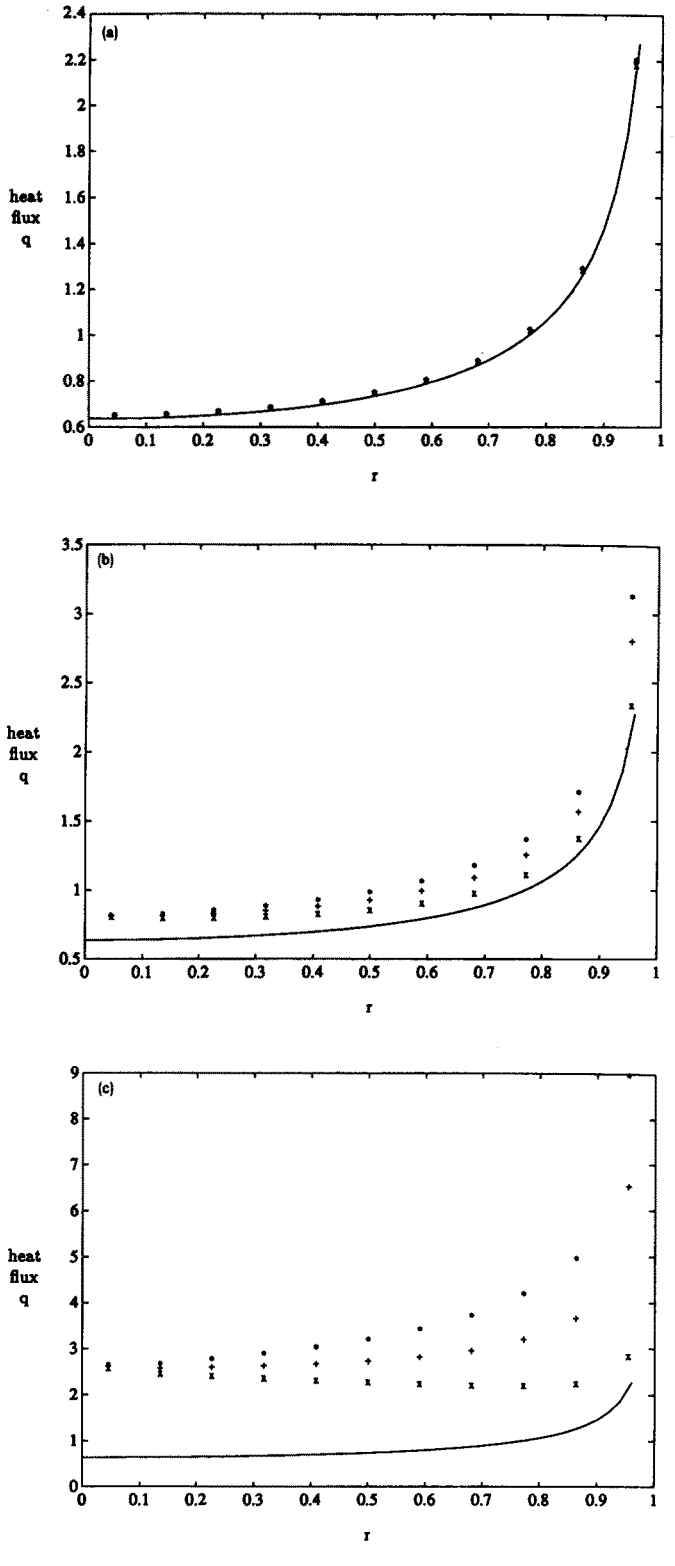

FIG. 5. The heat flux distribution over a circular disk as a function of Peclet number. (a) $P = 0.01$; (b) $P = 1.0$; and (c) $P = 100.0$; *: leading edge; +: side edge; and ×: trailing edge; solid line is the conduction solution $P = 0$.

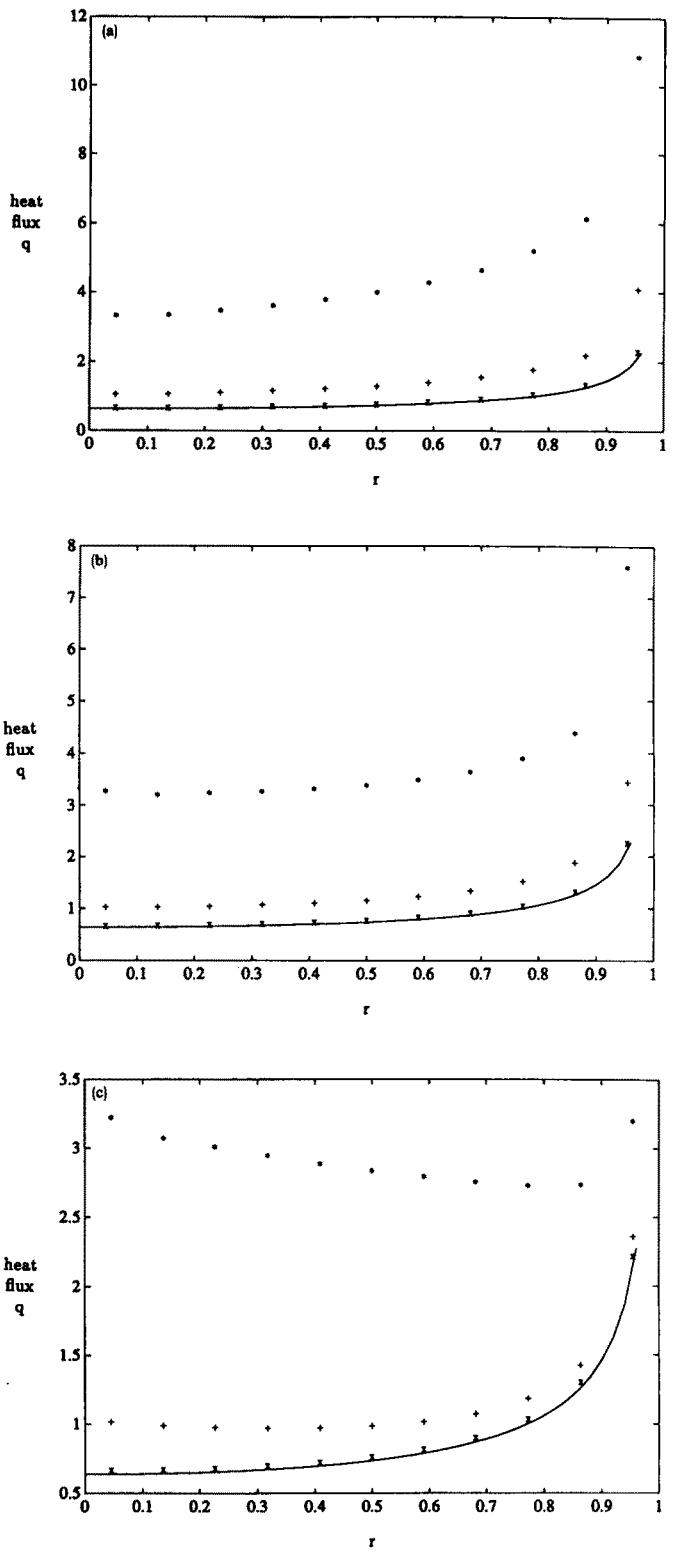

FIG. 6. The effect of Peclet number on heat transfer over different regions of a circular disk. (a) leading edge; (b) side edge; (c) trailing edge; ×: $P = 0.04$; +: $P = 4.0$; and *: $P = 200.0$; solid line is the conduction solution.

ciently that the heat transfer, driven by a temperature difference between the surface and the bulk fluid, diminishes over almost the entire length of the central region of the film.

In Figs. 6(a)–6(c) we compare the heat transfer that occurs over different regions of the disk as a function of Peclet number. In these figures the symbols,* +, and × correspond to Peclet numbers 0.04, 4.0, and 200.0, respectively. The solid line again is the conduction solution. Near the leading edge, we find the expected result that increasing the Peclet number substantially increases transport from the

surface. Over the center of the disk there is only a moderate variation of the heat flux until near the edge where the square root singularity is important. This relative insensitivity in the transverse direction, together with the large fluxes over the majority of the heated surface that are characteristic of higher Peclet numbers, suggest that a two-dimensional approximation may be useful for $P \gg 1$. Nevertheless the very large fluxes characteristic of the edge regions clearly make 3-D effects important. Around the trailing edge, the high Peclet number preheating, as mentioned in Sec. IV A, is evident and at $P = 200.0$ the heat flux distribution has a sharp minimum.

C. Total heat transfer as a function of Peclet number

The total heat transfer (Nusselt number) as a function of Peclet number is important in the design of a heat flux probe. Kalumuck[5] presented the first complete treatment for rectangular probes imbedded in conducting substrates, assuming that the boundary condition is one of a prescribed uniform heat flux. The complete heat transfer curve for isothermal circular disks is shown in Fig. 7. In this figure the solid line represents numerical calculations covering more than five orders of magnitude of Peclet number. The symbols ($\times$) represent the theoretical low Peclet number result derived by Phillips,

$$N = (4.0 - 0.112\,68P^{3/2})/(1.0 - 0.202\,81P^{1/2}) \quad (12)$$

and, clearly, is remarkably accurate up to Peclet numbers $O(1)$. The long dashed line is the high Peclet number asymptote $N = 2.157P^{1/3} + O(P^{-1/6})$,[21] which is derived by integrating the 2-D boundary layer solution (called the Leveque solution) for strips over the disk. The $P^{-1/6}$ error term given is the correction because of the leading and trailing edge regions where the heat flux undergoes a jump discontinuity.[4,10] It is evident that the one-term high-Peclet-number approximation becomes accurate within 5% when $P > 400.0$.

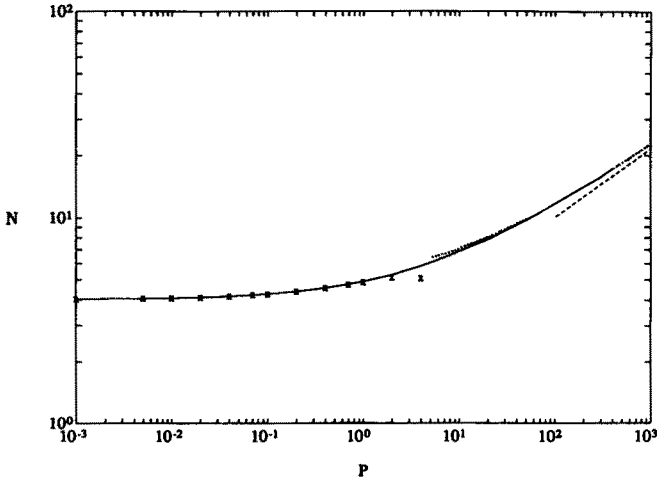

FIG. 7. Heat transfer from isothermal circular films: Nusselt number as a function of Peclet number. Numerical results are given by the solid curve. $\times$: Phillips[4] low Peclet number asymptotic formula, Eq. (12);—: $N = 2.157\,P^{1/3}$; $\cdots$: Eq. (13).

The short dashed line shown in Fig. 7 is a proposed correction for high Peclet numbers

$$N = 2.157P^{1/3} + 3.55P^{-1/6}. \quad (13)$$

The constant 3.55 is calculated from the numerical results at $P = 100.0$ and 200.0.[22] In Fig. 7 this approximation is extrapolated to higher Peclet numbers to illustrate the rate of approach to the simple one-term estimate. Remarkably, this simple correction also lies within 3% of the numerical results for Peclet numbers as low as $P = 10.0$ and within 7% at $P = 5.0$. Since many applications involve flow conditions such that $P = O(1)$, it is hoped that both the "exact" numerical results and the simple correlation (13) may prove to be of some value.

V. NUMERICAL RESULTS: ELLIPTICAL FILMS

In this section we summarize our numerical results for isothermal elliptical disks aligned parallel and perpendicular to the flow direction. The Nusselt number versus Peclet number "design" curves are reported for aspect ratios 0.2–5.0 and the question of arbitrary probe orientation is addressed using the numerical simulations in conjunction with an analytic result valid at high Peclet numbers.

The numerical procedure is practically identical to that used for circular disks. For noncircular films it is common and physically meaningful to use the disk dimension in the direction of flow as the characteristic length scale. However, this implies that a variation in the probe orientation changes the Peclet number. Since one goal of this study is to assess variations of heat flow for different disk orientations relative to the bulk flow, we introduce a characteristic length such that a change in orientation results in no change to the Peclet number and, at most, may alter the Nusselt number. Hence, for an ellipse with semiaxes a,b in the x,y directions, respectively, we define $l = \sqrt{ab}$ and the dimensionless ellipse boundary is described by $\beta x^2 + (1/\beta)y^2 = 1$, where the aspect ratio β is defined as $\beta = b/a$. By definition, $\beta < 1$ corresponds to slender elliptical films aligned in the flow direction. The dimensionless area of the elliptical disk is π.

In the case of an isothermal elliptical disk imbedded in an adiabatic boundary, the conductive heat flux is given by (Landau and Lifshitz[20])

$$q_c = \mathbf{n}\cdot\nabla T = f(\beta)1/\left[\sqrt{1 - \beta x^2 - (1/\beta)y^2}\right]. \quad (14)$$

The coefficient $f(\beta)$ is given by

$$f^{-1}(\beta) = \frac{1}{2}\int_0^\infty \frac{dt}{\sqrt{(t+\beta)(t+1/\beta)t}}$$

$$= \sqrt{\beta}\,K(1-\beta^2), \quad (15)$$

where $K(1-\beta^2)$ is the complete elliptic integral of the first kind and this last equality requires $\beta \leqslant 1$ [for $\beta > 1$ simply replace β in Eq. (15) by $1/\beta$]. The total heat transfer in this case is $N = 2\pi f(\beta)$. Equation (14) also gives a square root singularity of the heat flux at the boundary.

The numerical results described below are obtained using method (ii) of Sec. III with the conductive heat flux, as given by Eq. (14). The film surface is subdivided into 11 concentric ellipses and also subdivided equally into 17 angular elements in order to resolve slender films accurately.

A. Effects of aspect ratio and Peclet number

We first consider the axisymmetric cases where the disk axes are aligned parallel and perpendicular to the flow direction. These two situations correspond to axis ratios β and $1/\beta$, respectively. Examining the total heat transfer for the two orthogonal orientations yields the maximum possible measurement error resulting from the misalignment of the heated element.

The Nusselt number as a function of the aspect ratio is reported for different values of the Peclet number $0.01 \leqslant P \leqslant 100.0$ in Fig. 8 and the figure insets show the respective disk orientations relative to the flow. The solid curves are the numerical results and the dashed lines are an asymptotic high Peclet number approximation, which is discussed below. At a given P, orientation effects are negligible if the curves $N(\beta;P)$ are symmetric about $\beta = 1.0$. For $P < 0.1$, we see from Fig. 8 that effects of disk orientation are indeed negligible and, although the total heat transfer is a function of aspect ratio, $N(\beta)$ differs from $N(1/\beta)$ by less than 1%. At $P = 1.0$ there is only a 2% difference between $N(\beta)$ and $N(1/\beta)$. For small Peclet numbers the minimum near $\beta = 1$ is a consequence of the high fluxes resulting from the square root singularity near the edge coupled with the smaller film circumferences as $\beta \to 1$.

In Fig. 8, as the Peclet number is increased above $O(1)$ the minimum in the curves $N(\beta;P)$ shifts to smaller β. For $P > 40$ the total heat transfer is a monotonic increasing function of aspect ratio for $\beta \geqslant 0.2$. Physically this corresponds to increased heat transfer as the length of the leading edge of the heated film is increased. Hence the maximum error incurred because of the misalignment of slender probes (say $\beta > 4$) increases to 10% at $P = 10$, 17% at $P = 40$, and is greater than 20% at $P = 100$. For nearly circular disks ($\beta \approx 1$) the misalignment error will clearly be smaller.

For high Peclet numbers $P > 100$, long computation times and the excessive computer storage necessary to store a large array have prevented us from accurately generating the necessary Green's function for very slender films. However, the numerical results do indicate that the Nusselt number increases as the aspect ratio increases for the higher values of Peclet numbers illustrated in Fig. 8. The dashed lines in Fig. 8 represent an approximate high Peclet number result calculated from the 2-D boundary layer theory that predicts $N \approx P^{1/3}\beta^{1/6}$ (see Sec. V B below) and based on our results for circular disks we may expect this approximation to be useful for $P > 400$ (for restrictions on the applicability of this boundary layer estimate, refer to Sec. V B).

In Fig. 9 we present results of N as a function of P for aspect ratios $\beta = 0.25$, 0.5, 2.0, and 4.0. As discussed above, at low Peclet numbers the total heat transfer is conduction dominated and is predominantly a function of aspect ratio alone, being the same for β and $1/\beta$ since these simply correspond to orthogonal orientations. As the Peclet number is increased above $P > 8$, convective transport plays a more significant role, so that probe orientation becomes important. Hence for $P > 40$ the surface film with the longest leading edge (largest β) transfers the most heat.

B. Arbitrary orientation at high Peclet numbers

For the case where the disk has an arbitrary orientation with respect to the flow, it is possible to determine the first term in an asymptotic expansion at high Peclet numbers. As just illustrated in Figs. 8 and 9, the largest measurement errors resulting from misalignment will occur for slender probes. Let ϕ denote the angle between the flow direction and the major ($\bar{x}$) axis of the film. For clarity in the discussion below we assume $\beta < 1$ as ϕ varies $0 \leqslant \phi \leqslant \pi/2$. The lengths along the disk axes are then $\beta^{-1/2}$ and $\beta^{1/2}$. We assume that for sufficiently large values of the Peclet number, the dominant contribution to the total heat transfer takes place over the central portion of the probe. Then the Nusselt number can be calculated by integrating the 2-D Leveque result over the surface of the oriented ellipse.[23] The result may simply be expressed as

$$N(\beta,P) \sim \left[3(6^{1/3})\Gamma\left(\tfrac{1}{3}\right)/5\Gamma\left(\tfrac{2}{3}\right)\right] P^{1/3}\beta^{1/6}\left[\cos^2(\phi) + (1/\beta^2)\sin^2(\phi)\right]^{1/6}. \quad (16)$$

Crudely, the dependence on $\beta^{1/6}$ follows as the product of (1) net heat transfer from a strip of the surface in the flow direction, $O(\beta^{-1/3})$ and (2) the cross-sectional length of

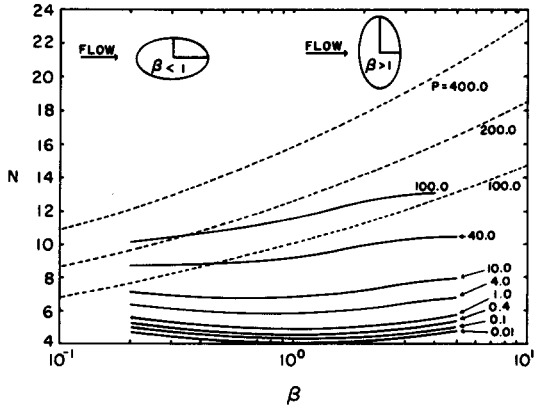

FIG. 8. Heat transfer from elliptical films: Nusselt number as a function of aspect ratio for different Peclet numbers. Solid curves are the numerical simulations. Dashed curves are a high Peclet number asymptotic result, $N \approx P^{1/3}\beta^{1/6}$ [Eq. (16)].

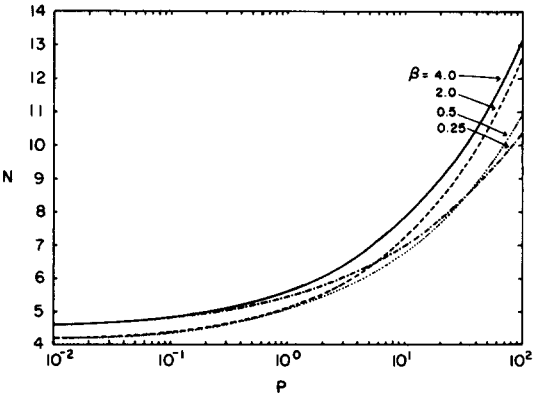

FIG. 9. Heat transfer from elliptical films: Nusselt number as a function of Peclet number for different aspect ratios $\beta = 0.25$, 0.5, 2.0, and 4.0.

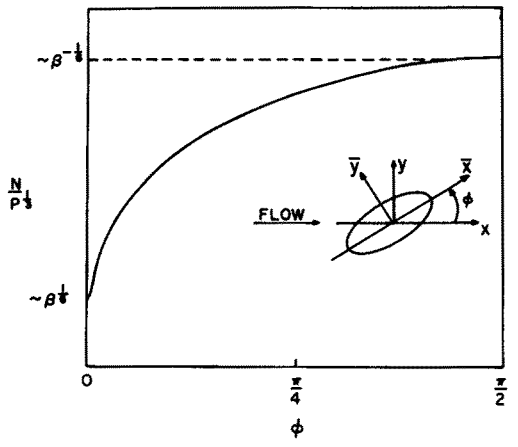

FIG. 10. The effect of orientation on heat transfer from slender elliptical films. The solid curve is a qualitative plot of Eq. (16) that illustrates the change from heat transfer proportional to $\beta^{1/6}$ to the more efficient $\beta^{-1/6}$ $\times(\beta<1)$ as more of the leading edge is exposed to the flow.

the ellipse perpendicular to the flow direction $O(\beta^{1/2})$. For ellipses aligned parallel and perpendicular to the flow, this result was compared with the numerical simulations in Fig. 8.

The approximation (16) shows that for slender ellipses aligned with the flow (small ϕ) the heat transfer decreases as the slenderness increases, although it only decreases as the one-sixth power of the aspect ratio. It also clearly illustrates the importance that even small rotations ($\phi>\beta$) may have in substantially increasing film transport. This occurs by exposing more of the leading edge of the probe to the flow, thereby effectively changing the total heat transport from dependence on $\beta^{1/6}$ to $\beta^{-1/6}$ ($\beta<1$). This effect is illustrated qualitatively in Fig. 10.

Calculation of the total heat transport using boundary layer concepts provides a valid first approximation as long as the total flux from the edge regions, where conduction is important, is negligible. The edge contribution has been mentioned earlier and is difficult to estimate in the general case. However, roughly speaking, the edge regions produce a total flux that is the product of an $O(1)$ constant and the total film circumference, which is $O(\beta^{-1/2})$. Hence for (16) to be valid for slender films aligned with the flow $\phi\to 0$, we require ($\beta<1$)

$$O(P^{1/3}\beta^{1/6})\gg O(\beta^{-1/2})\to P\gg\beta^{-2},$$

while for slender films oriented perpendicular to the flow, $\phi\to\pi/2$,

$$O(P^{1/3}\beta^{-1/6})\gg O(\beta^{-1/2})\to P\gg\beta^{-1}.$$

ACKNOWLEDGMENTS

The author would like to take this opportunity to extend a special thanks to Dr. John Hinch for suggesting this problem and for providing valuable advice throughout the course of this work. Discussions with Professor Joe Keller and Dr. Christopher Phillips were also very beneficial.

This work was funded through a NSF–NATO Postdoctoral Fellowship awarded to the author for study at the Department of Applied Mathematics and Theoretical Physics, University of Cambridge, Cambridge, England.

APPENDIX: ANALYTIC TREATMENT OF THE SINGULARITY IN THE FUNCTION g

In this appendix we describe the analytic treatment of the singularity in the function g. The singular behavior occurs at the origin in λ space and is handled by integrating over a circular region of radius ϵ, S_ϵ. So, we have

$$g(\mathbf{x}_s,\xi;P) = -\int_{S_\epsilon}\exp^{[-i\lambda\cdot(\xi-\mathbf{x}_s)]}\frac{\mathrm{Ai}(s)}{(iP\lambda_x)^{1/3}\mathrm{Ai}'(s)}\times d\lambda_x\,d\lambda_y - \int_{S_\epsilon}\frac{1}{\sqrt{\lambda_x^2+\lambda_y^2}}\,d\lambda_x\,d\lambda_y. \quad (A1)$$

The second integral is straightforward to evaluate and equals $2\pi\epsilon$. The first integral is evaluated asymptotically by first transforming to cylindrical coordinates $\lambda_x=\rho\cos\theta$, $\lambda_y=\rho\sin\theta$ and expanding the integrand for large and small values of the argument $(\rho^2/P\cos\theta)^{1/3}$,

$$\frac{\mathrm{Ai}[\rho^{4/3}/(iP\cos\theta)^{2/3}]}{(iP\cos\theta)^{1/3}\mathrm{Ai}'[\rho^{4/3}/(iP\cos\theta)^{2/3}]} \sim\begin{cases}-(c_1/c_2)/(iP\rho\cos\theta)^{1/3}, & \text{for } \rho^2/P<|\cos\theta|;\\ -1/\rho, & \text{for } \rho^2/P>|\cos\theta|,\end{cases} \quad (A2)$$

where c_1 and c_2 are constants that arise in the series representation of the Airy function,[19] $c_1=0.355\,028...$, and $c_2=0.258\,819...$. The upper expression in (A2) is valid for all θ, except near $\theta\approx\mp\pi/2$. It follows that there is negligible error in using the upper expression over the entire interval $0\leqslant\theta\leqslant 2\pi$ since, for example,

$$\int_0^\epsilon\int_{\pi/2-\rho^2/P}^{\pi/2+\rho^2/P}\left(\frac{1}{\rho}\right)\rho\,d\rho\,d\theta\sim O(\epsilon^3).$$

Hence, provided $|\mathbf{x}_s-\xi|<\epsilon^{-1}$, the first integral in (A1) is asymptotically given by

$$\left(\frac{c_1}{c_2}\right)\int_0^\epsilon\int_0^{2\pi}\frac{1}{(iP\rho\cos\theta)^{1/3}}\rho\,d\rho\,d\theta. \quad (A3)$$

Integration yields

$$g\sim -2\pi\epsilon-\left(\frac{c_1}{c_2}\right)\frac{3\cdot 3^{1/2}}{5\cdot 2^{1/3}}\frac{\Gamma(\frac{1}{3})^2}{\Gamma(\frac{2}{3})}\left(\frac{\epsilon^5}{P}\right)^{1/3} \quad (A4)$$

or

$$g\sim -2\pi\epsilon-5.996\,57(\epsilon^5/P)^{1/3}.$$

[1]T. J. Hanratty and J. A. Campbell, in *Fluid Mechanics Measurements*, edited by R. J. Goldstein (Hemisphere, Washington, 1983).
[2]T. J. Pedley, *The Fluid Mechanics of Large Blood Vessels* (Cambridge U.P., Cambridge, 1980).
[3]A. M. Kraynik and W. R. Schowalter, J. Rheology **25**, 95 (1981).
[4]C. G. Phillips, Q. J. Mech. Appl. Math. (in press).
[5]K. M. Kalumuck, Ph.D. thesis, Massachusetts Institute of Technology, 1983.
[6]R. C. Ackerberg, R. D. Patel, and S. K. Gupta, J. Fluid Mech. **86**, 49 (1978).
[7]S. C. Ling, J. Heat Transfer, Trans. ASME C **85**, 230 (1963).
[8]J. Newman, in *Electroanalytical Chemistry*, edited by A. J. Bard (Dekker, New York, 1973), Vol. 6, p. 187.
[9]S. G. Springer and T. J. Pedley, Proc. R. Soc. London Ser. A **333**, 347 (1973).

[10]S. G. Springer, Proc. R. Soc. London Ser. A **337**, 395 (1974).
[11]It should be noted that the expressions for the total heat flux from two-dimensional strips given by Ling[7] and Springer[10] are incorrect at all but the leading order since, in their analysis of the trailing edge, they failed to include comparable contributions from the leading edge and the boundary layer regions. Phillips[4] derived a corrected expression.
[12]L. P. Reiss and T. J. Hanratty, AIChE J. **9**, 154 (1963).
[13]J. D. Jackson, *Classical Electrodynamics* (Wiley, New York, 1962).
[14]M. A. Leveque, Ann. Mines **13**, 201 (1928).
[15]The flux has been nondimensionalized with respect to k/l where k is the thermal conductivity of the fluid.
[16]L. C. Wrobel and C. A. Brebbia, in *Numerical Methods in Heat Transfer*, edited by R. W. Lewis, K. Morgan, and O. C. Zienkiewicz (Wiley, New York, 1981), p. 91.
[17]E. O. Brigham, *The Fast Fourier Transform* (Prentice–Hall, Englewood Cliffs, NJ, 1974).
[18]W. H. Press, B. P. Flannery, S. A. Teukolsky, and W. T. Vetterling, *Numerical Recipes* (Cambridge U.P., Cambridge, 1986).
[19]M. A. Abramowitz and I. A. Stegun, *Handbook of Mathematical Functions* (Dover, New York, 1968).
[20]L. D. Landau and E. M. Lifshitz, *Electrodynamics of Continuous Media* (Pergamon, Oxford, 1960).
[21]The exact expression for the first term is $N = [3(6^{1/3})\Gamma(\frac{1}{3})/5\Gamma(\frac{2}{3})]P^{1/3}$, where Γ is the Gamma function.
[22]The analysis of Phillips[4] indicates an additional $O(P^{-1/5})$ contribution to the heat flux from the side edges of the film. It is clear that Eq. (13) represents a useful approximation over a large range of Peclet numbers, rather than providing the actual coefficient of the $P^{-1/6}$ term.
[23]From boundary layer theory, the flux from a streamwise strip of length L is $[3^{4/3}P^{1/3}/2\Gamma(\frac{1}{3})]L^{2/3}$.